Supporting information

Programmable Atomic Neighborhoods in Copper Rewire the Oxygenate Pathway to Ethanol

Chi-Wei Chou [a, †], *Ding-Huei Tsai* [a, †], *Ying-Rui Lu* [b], *Yung-Jung Chuang* [c], *Yung-Tin (Frank) Pan* [a], *Tsu-Chin Chou* [c,d], *Wei-Shun Chang* [e] *and Hsing-Yu Tuan* [a, f, *]

C.-W. Chou, D.-H. Tsai, Y.-R. Lu, Y.-J. Chuang, Y.-T. (Frank) Pan, T.-C. Chou, W.-S. Chang [e] *and, H.-Y. Tuan* [*]

[a] Department of Chemical Engineering, National Tsing Hua University, Hsinchu, 30013, Taiwan

[b] National Synchrotron Radiation Research Center, Hsinchu, 30076, Taiwan

[c] Institute of Analytical and Environmental Sciences, National Tsing Hua University, Hsinchu, 30013, Taiwan

[d] College of Sustainability, National Tsing Hua University, Hsinchu, 30013, Taiwan

[e] Department of Chemistry and Biochemistry, University of Massachusetts Dartmouth, 285 Old Westport Rd, North Dartmouth, MA 02747, United States

[f] Department of Chemical Engineering, Chung Yuan Christian University, Chungli, Taoyuan, 32023, Taiwan

Email: hytuan@che.nthu.edu.tw

†: These authors contributed equally to this work and share first authorship.

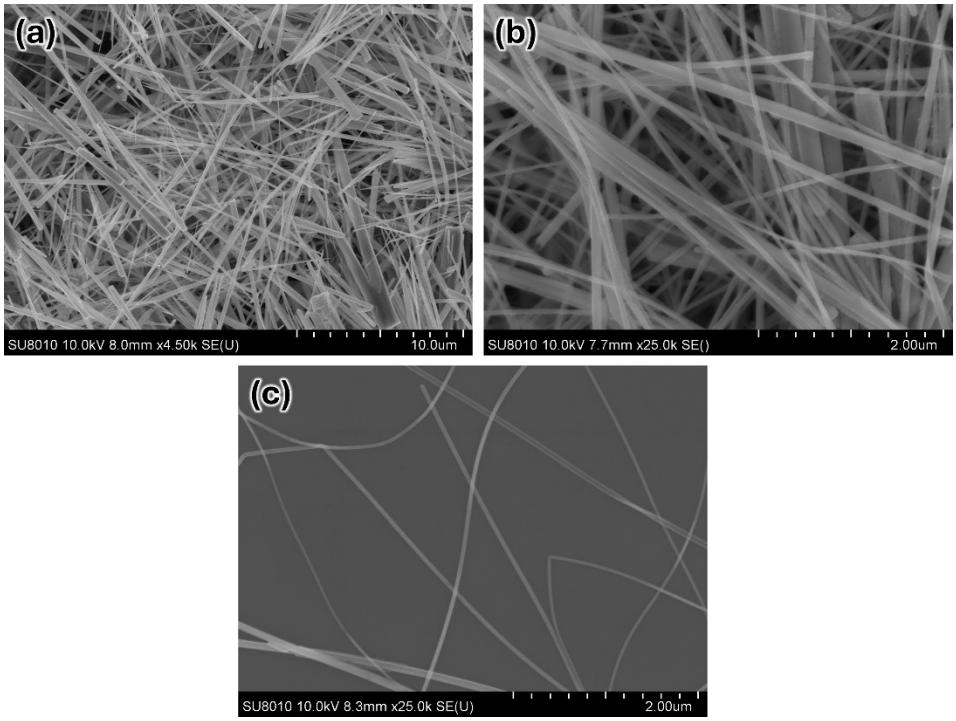

Figure S1. SEM pattern of Cu NWs.

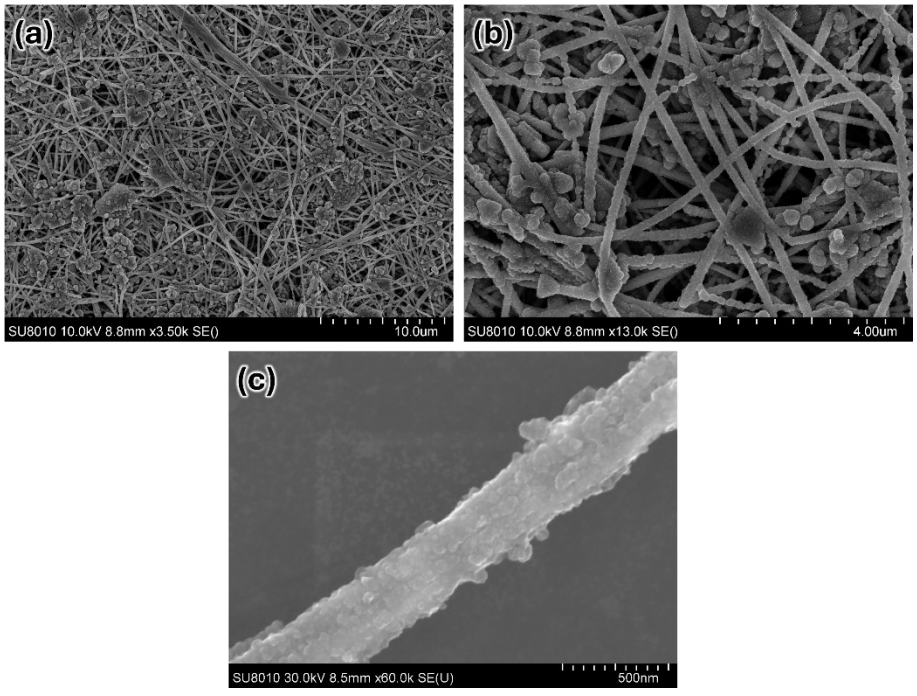

Figure S2. SEM pattern of cluster/Cu NWs.

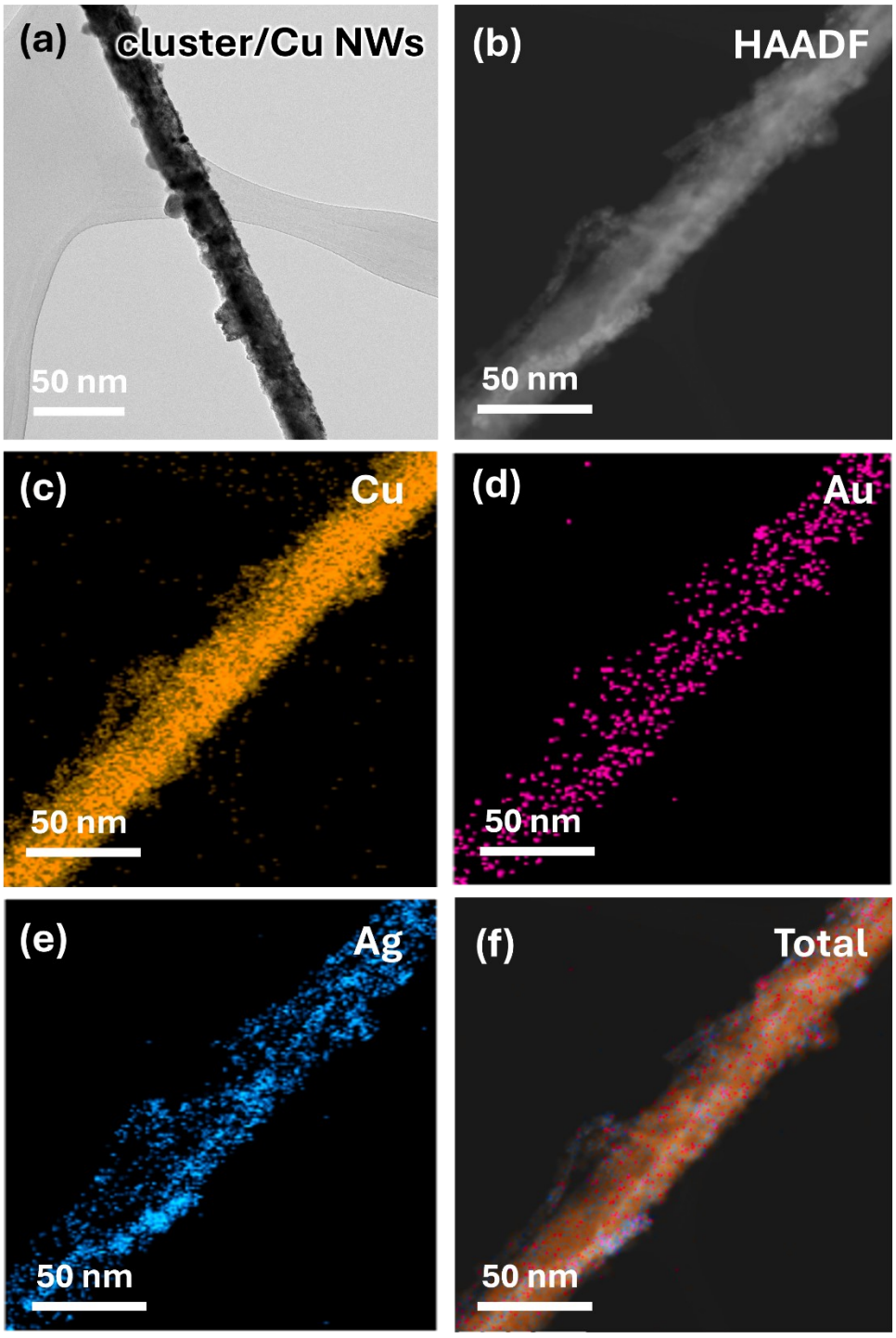

Figure S3. a) TEM images of cluster/Cu NWs. b) HAADF-STEM image c-f) corresponding EDS overlay mapping of cluster/Cu NWs, with elemental maps of Cu, Ag, and Au.

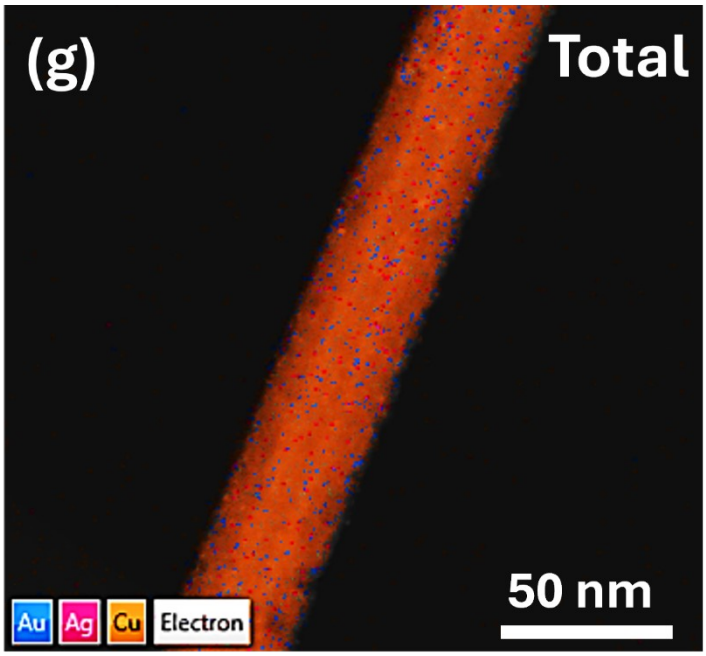

Figure S3. SEM pattern of cluster/Cu NWs.

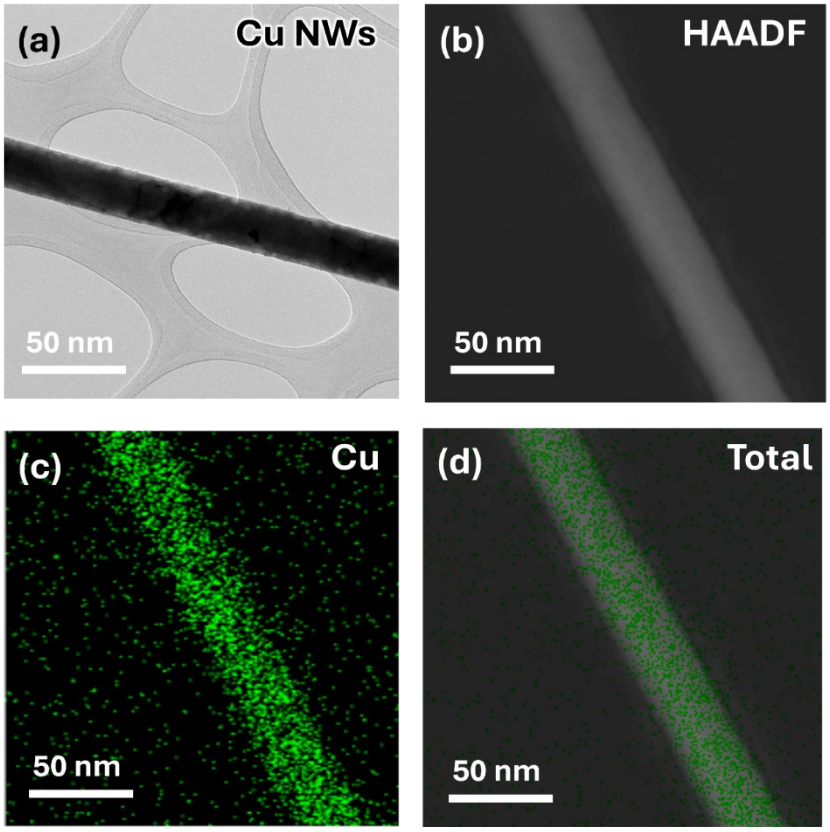

Figure S4. a) TEM images of Cu NWs. b) HAADF-STEM image c-d) corresponding EDS overlay mapping of Cu NWs, with elemental maps of Cu.

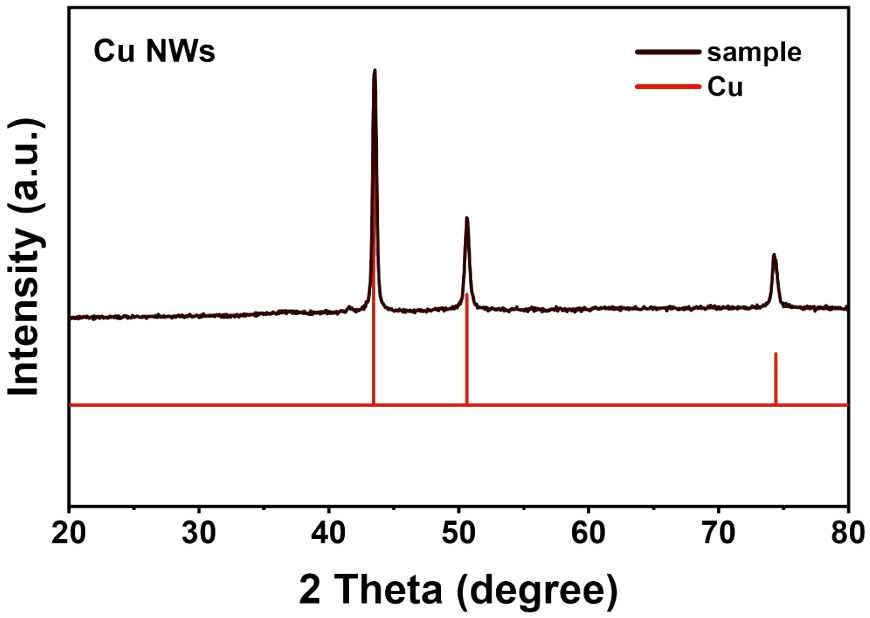

Figure S5. XRD pattern of Cu NWs.

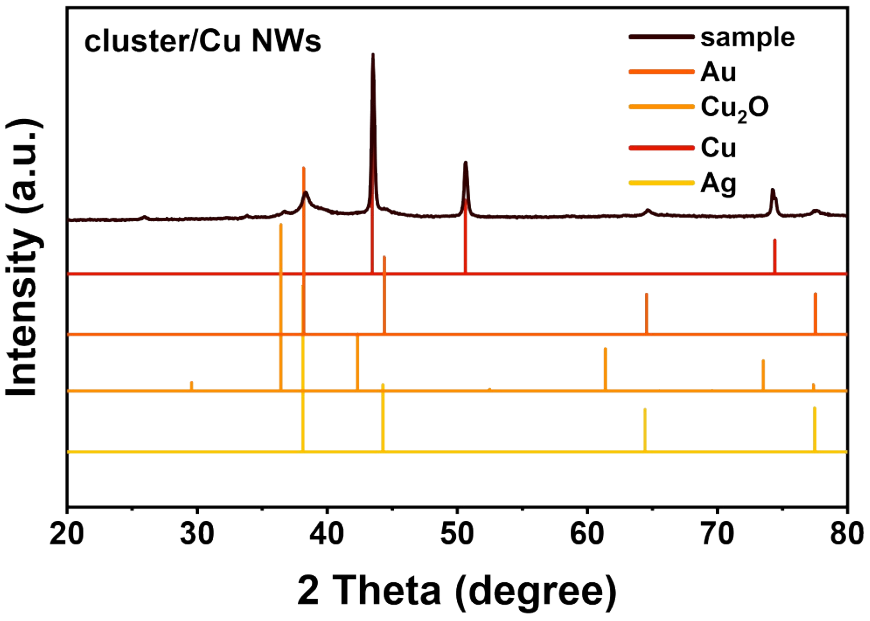

Figure S6. XRD pattern of cluster/Cu NWs.

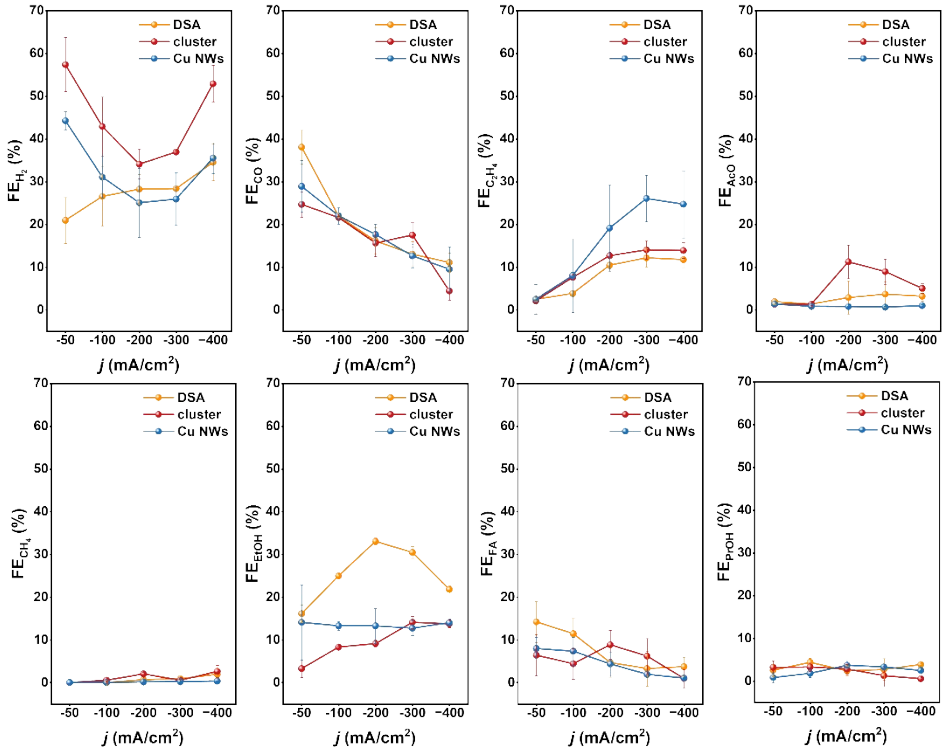

Figure S7. Faradaic efficiencies of major CO_2RR products (C_2^+, CO, C_2H_4, AcO^-, CH_4, EtOH, FA, and PrOH) as a function of the effective CO_2RR current density (j_{CO2RR}) for Cu NWs, cluster/Cu NWs, and DSA/Cu NWs.

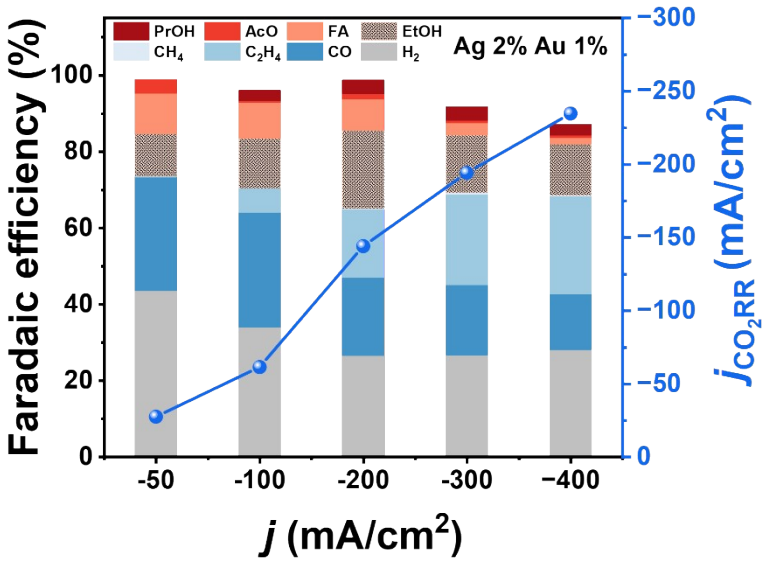

Figure S8. The effect operating current density on the FE of different products while using different ratio of Ag-Au (2% of Ag and 1% of Au) on Cu NWs.

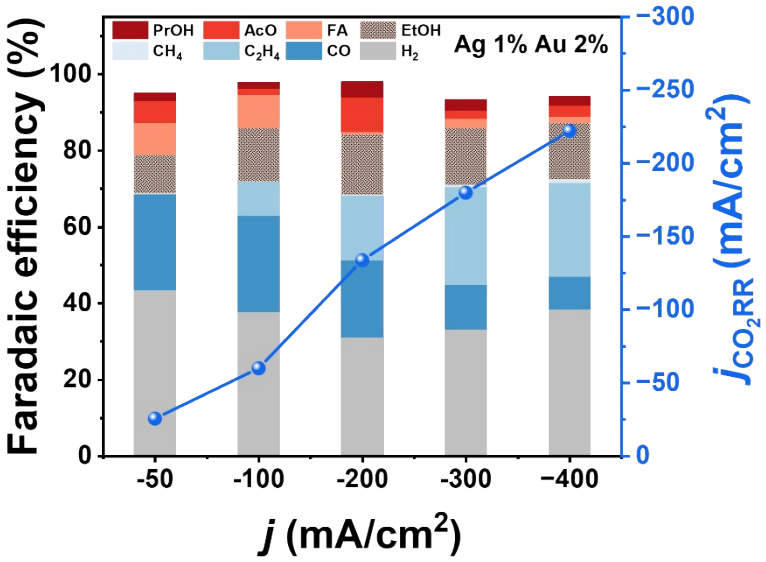

Figure S9. The effect operating current density on the FE of different products while using different ratio of Ag-Au (1% of Ag and 2% of Au) on Cu NWs.

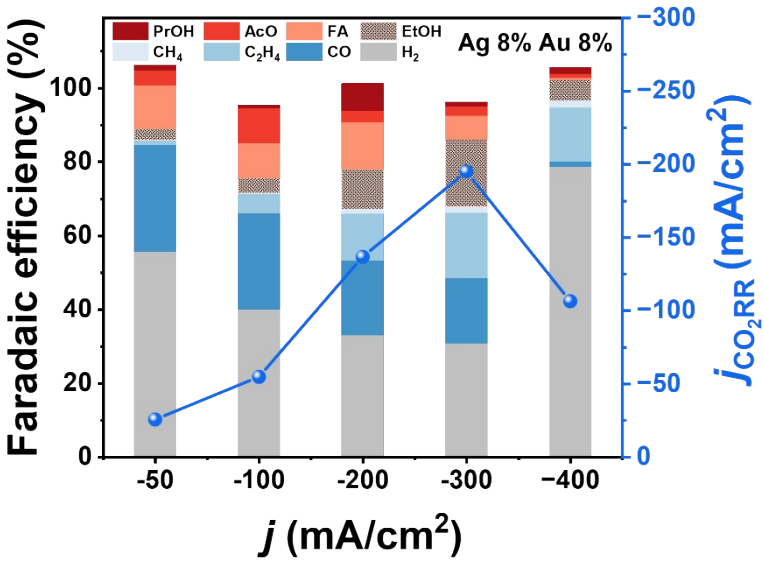

Figure S10. The effect operating current density on the FE of different products while using different ratio of Ag-Au (8% of Ag and 8% of Au) on Cu NWs.

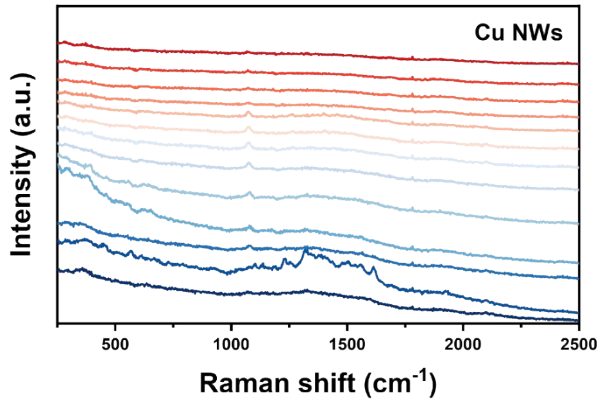

Figure S11. Potential-dependent operando Raman spectra of DSA/Cu NWs collected under stepwise cathodic biases during CO_2RR..

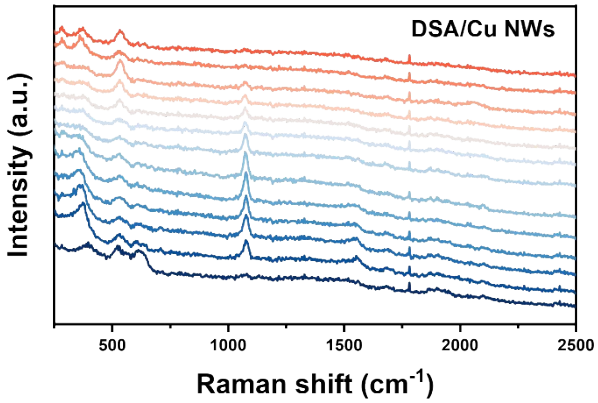

Figure S12. Potential-dependent operando Raman spectra of Cu NWs collected under stepwise cathodic biases during CO_2RR.

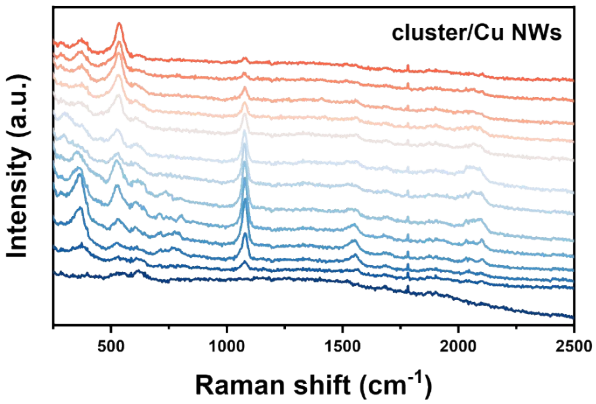

Figure 13. Potential-dependent operando Raman spectra of cluster/Cu NWs collected under stepwise cathodic biases during CO_2RR.

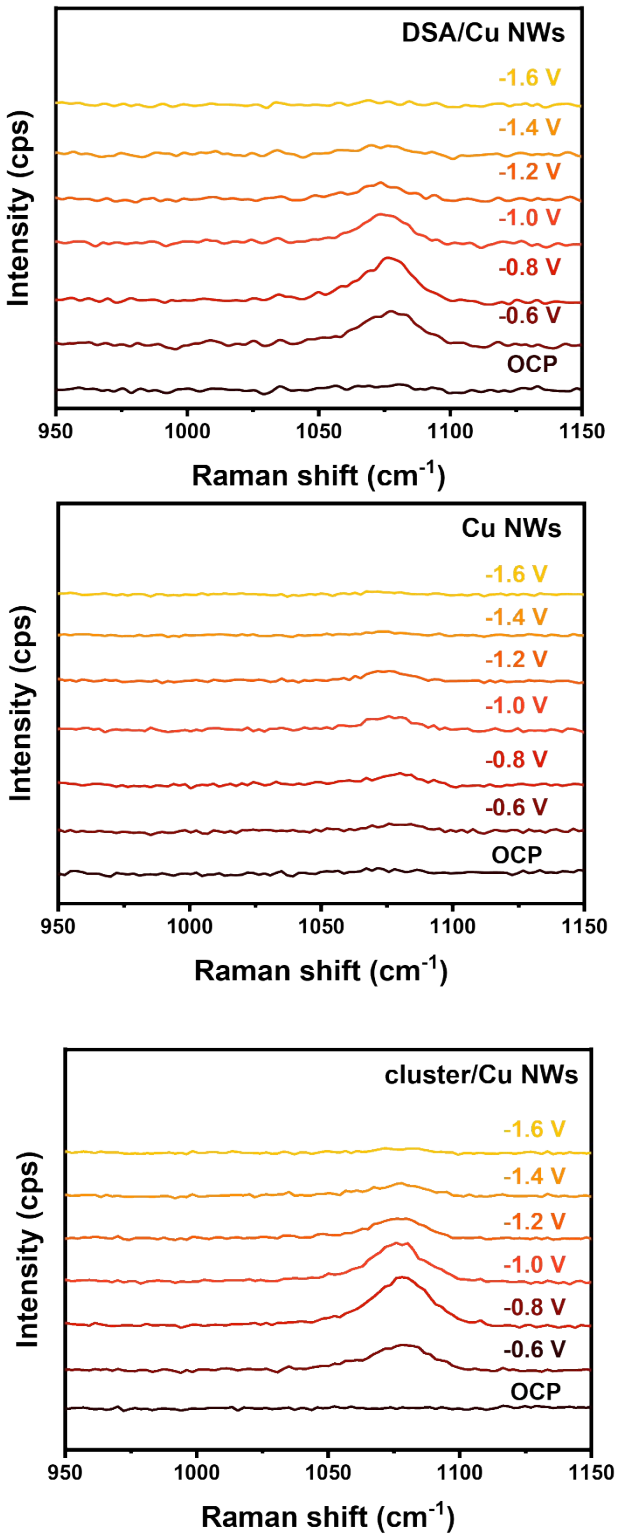

Figure S14. Potential-dependent operando Raman spectra (950–1150 cm^{-1}) of Cu NWs, DSA/Cu NWs, and cluster/Cu NWs collected under stepwise cathodic biases during CO_2RR.

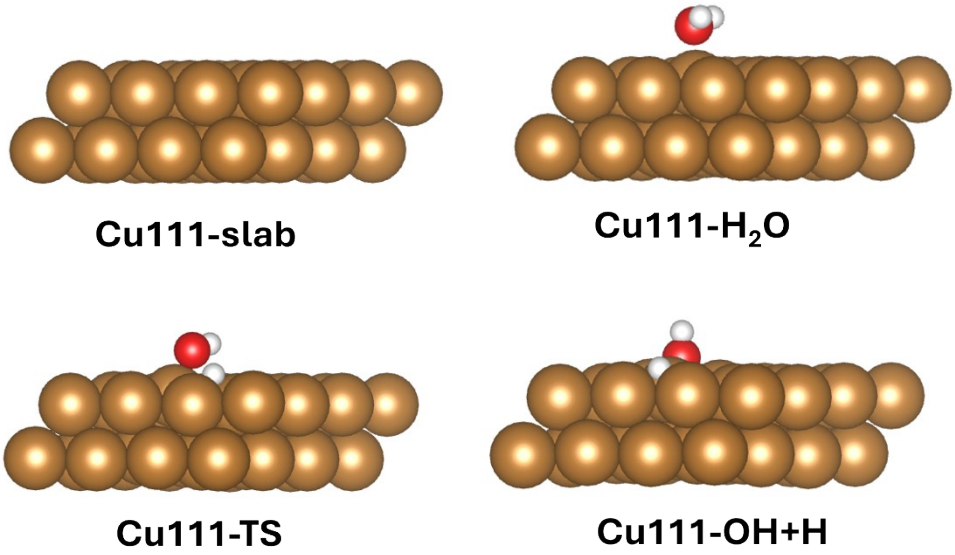

Figure S15. Optimized structural models of H_2O adsorption and stepwise dissociation ($*H_2O \rightarrow *OH + *H$) on Cu NWs.

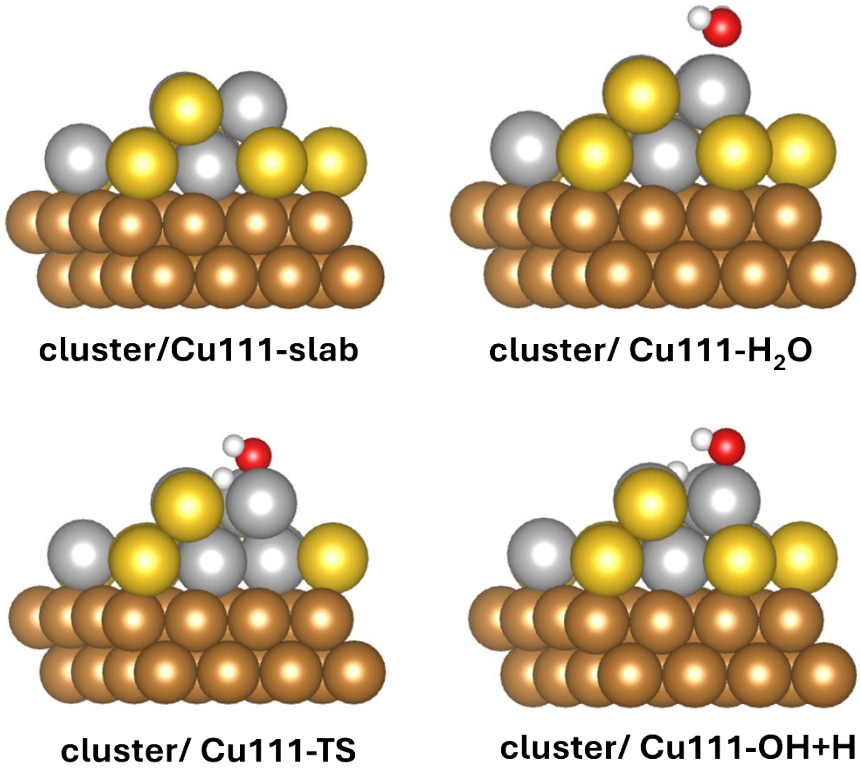

Figure S16. Optimized structural models of H_2O adsorption and stepwise dissociation ($*H_2O \rightarrow *OH + *H$) on cluster/Cu NWs.

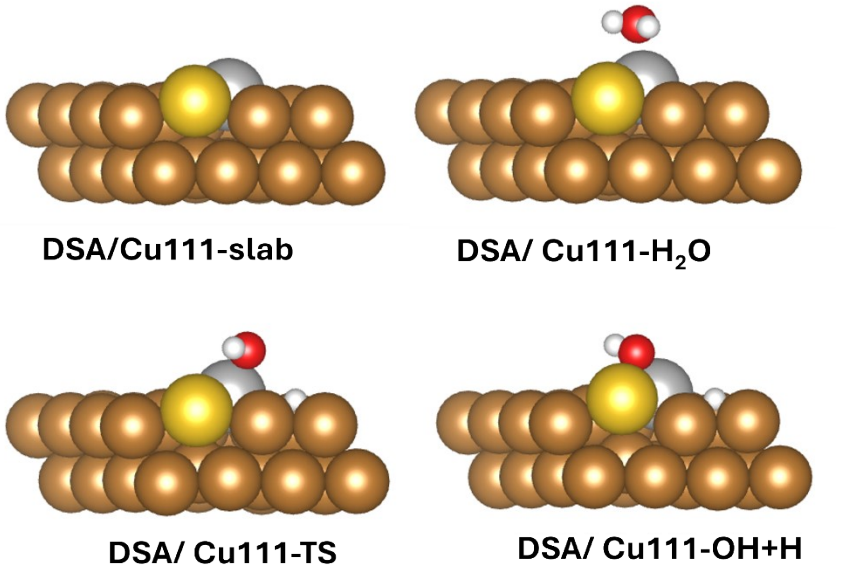

Figure S17. Optimized structural models of H_2O adsorption and stepwise dissociation ($*H_2O \rightarrow *OH + *H$) on DSA/Cu NWs.

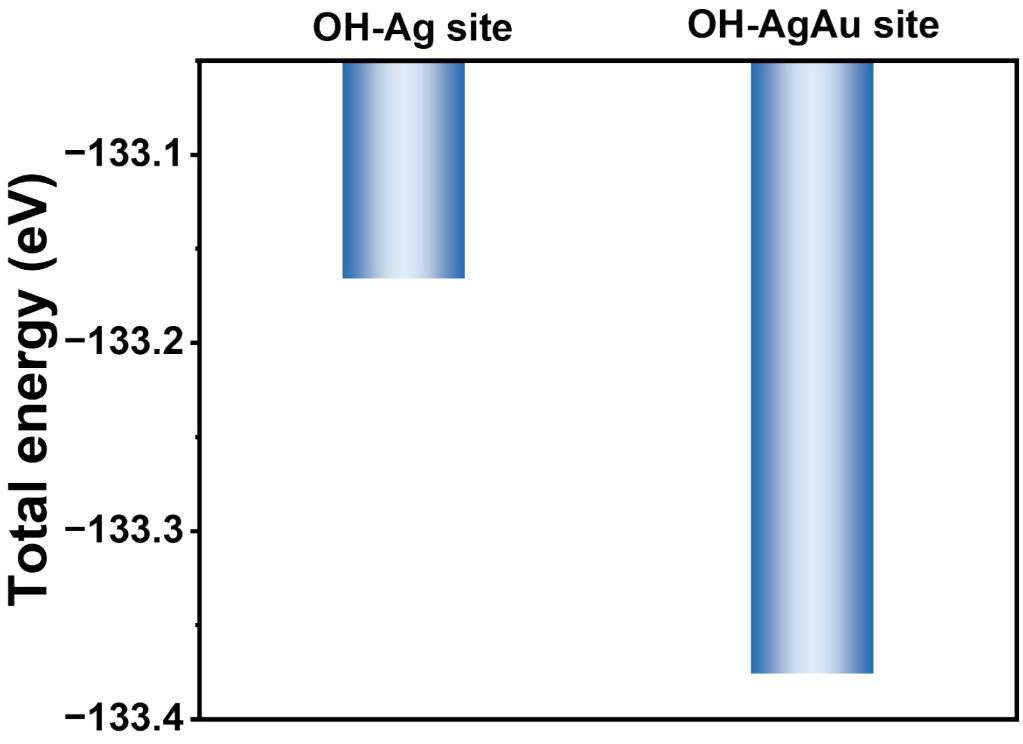

Figure S18. Calculated free-energy diagrams for H_2O adsorption DSA/Cu NWs surfaces.

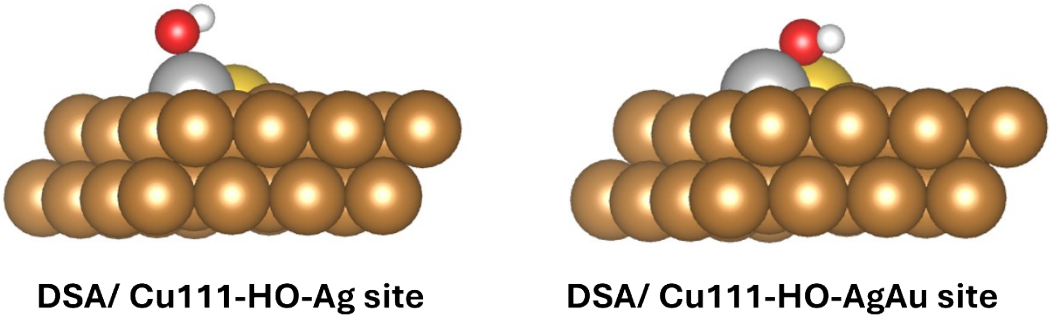

Figure S19. Optimized adsorption configurations of H_2O on DSA/Cu NWs surfaces.

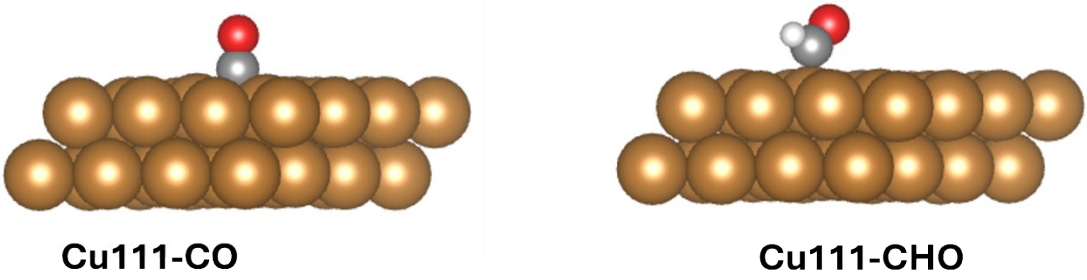

Figure S20. Optimized adsorption configurations of *CO on Cu(111)- modified surfaces.

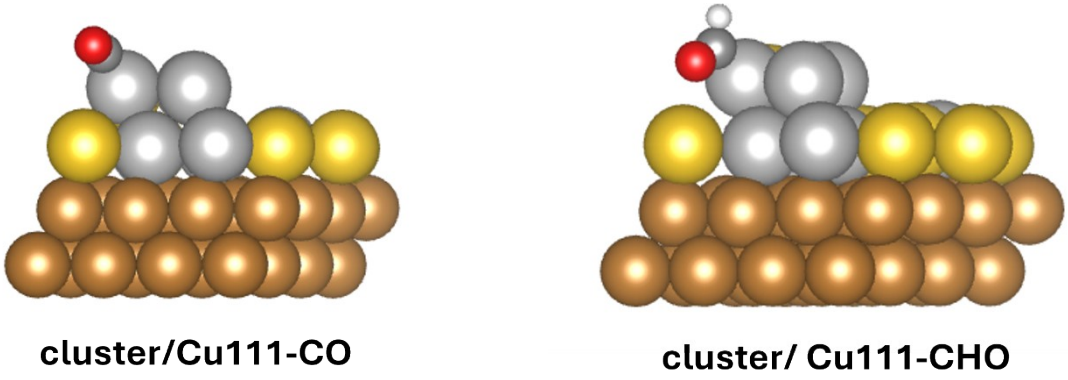

Figure S21. Optimized adsorption configurations of oxygenated intermediates on cluster-modified Cu(111) surfaces.

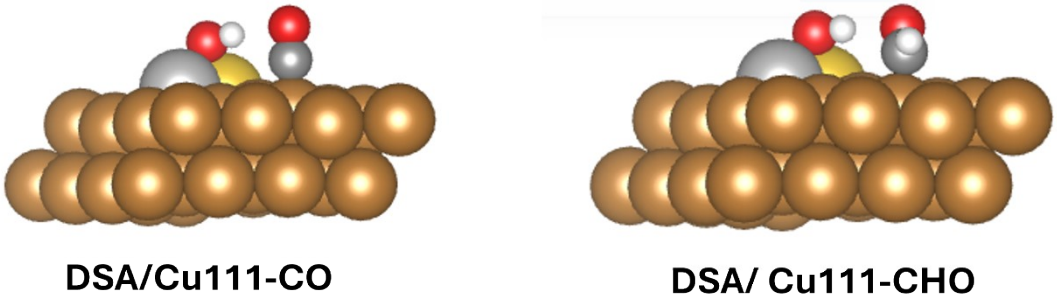

Figure S22. Optimized C–C coupling configurations (*CO–*CHO) on DSA-modified Cu(111) surfaces.

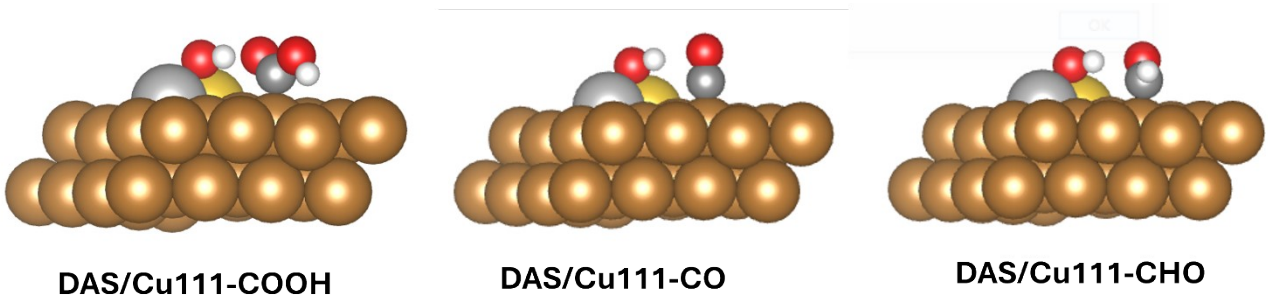

Figure S23. Optimized intermediates along the C1 hydrogenation pathway on DSA/Cu NWs.

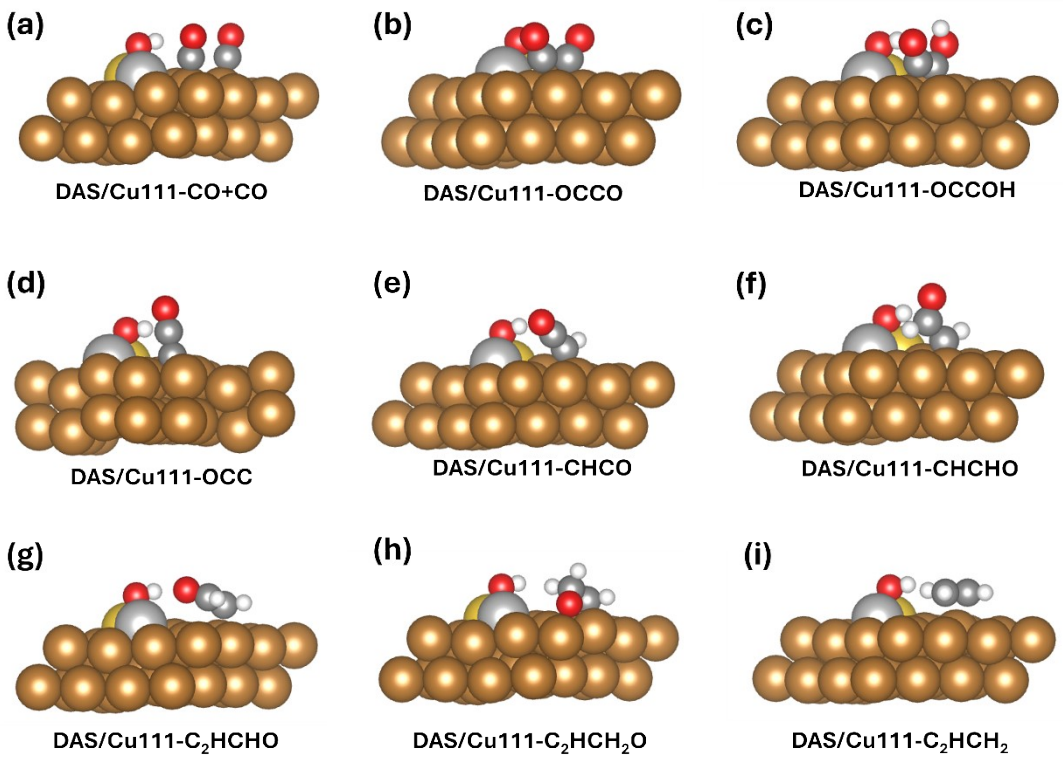

Figure S24. Optimized reaction intermediates along the C–C coupling pathway leading to ethylene formation on the catalyst surface.

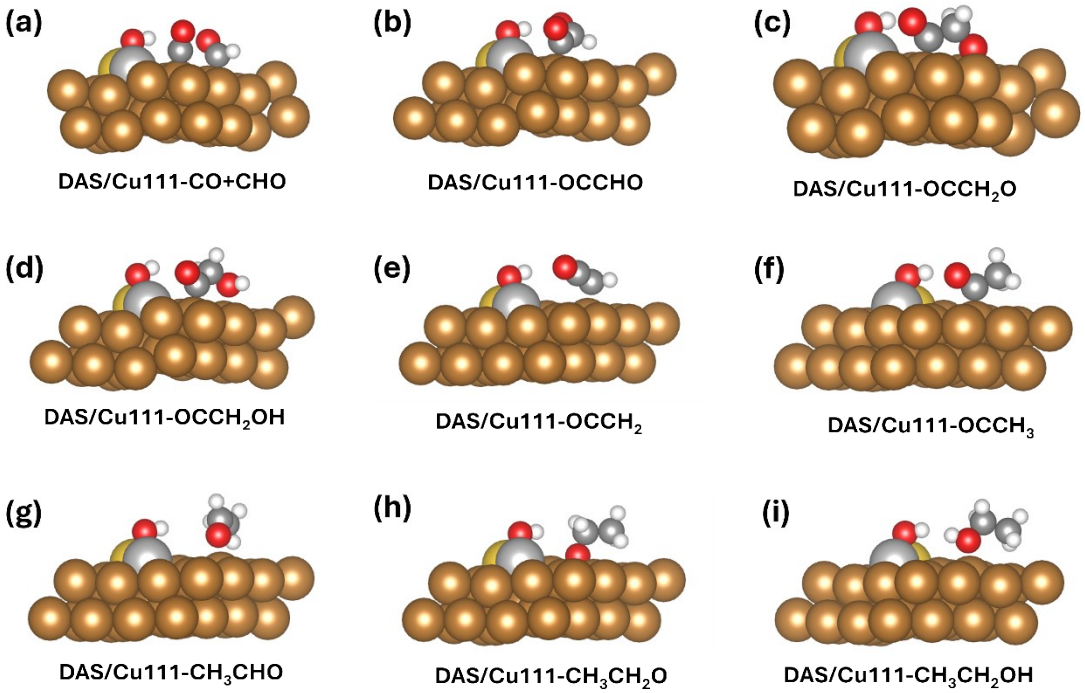

Figure S25. Optimized reaction intermediates along the C–C coupling pathway leading to ethanol formation on the catalyst surface.